FINAL REPORT DOE GRANT: DE-FG02-06ER46336 8/29/2005-5/15/2013
Institution: Rutgers University
Title: Atomistic Structure, Strength, and Kinetic Properties of Intergranular Films in Ceramics
PI: Stephen H. Garofalini

The research in this project addressed the detailed atomistic structure and behavior of intergranular films (IGFs) in alumina and silicon nitride ceramics using predominantly molecular dynamics computer simulation techniques, with correlations to HRTEM, AEM, ELNES, and HAADF-STEM experimental data. Additional work using ab-initio DFT calculations and developing and using atomic density function phase field calculations were also employed. A fundamental concept of the program has been that the effect of local structure and kinetics play a dominant role in behavior of the IGF. This concept now appears to be the basis of other programs studying IGFs in ceramics.

Later stages of the project concentrated on the very difficult problem of describing Lu siteing on the prism oriented surface of silicon nitride as seen in HAADF-STEM. Correct siteing of the two adsorption sites could not be achieved by other groups using ab-initio calculations but we were able to reproduce the HAADF-STEM in the simulations. Success in this specific effort provides information regarding the important role of oxygen replacing certain nitrogen surface lattice sites in silicon nitride and the required inclusion of the full IGF overlayer on this adsorption behavior.

Major results include:

(a) Predictions regarding the interfacial adsorption sites of network modifier ions in the silicate and silicon oxy-nitride IGFs onto specific crystal surfaces that were subsequently verified by electron microscopy techniques such as HAADF-STEM.

(b) The role of dissolution and growth of different crystal surfaces that show the competing processes of dissolution versus grain growth for specific surfaces as a function of temperature and provides an important mechanism for controlled processing of these materials.

(c) The role of the interface acting as a sink for particular species from the IGF; this affects segregation of species to the interface as dictated by the combined effect of the bonding characteristics of the segregants in the glass versus the segregants in the interface.

(d) The effect of this segregation of cations adsorbed to the surface described in (c) on attracting anions from the IGF and double-layer to multilayer formation on fracture behavior.

(e) Effect of rare earth ions, La and Lu, in silicon nitride IGFs on growth. While each of these rare earths is seen at the prism surface of silicon nitride in HAADF-STEM, potentially poisoning the surface, their affect on grain growth and other material properties is quite different. We have been able to provide the mechanism by which this occurs.

(f) Role of oxygen replacement of nitrogen at the crystal surface sites in silicon nitride on adsorption of La and Lu rare earth ions, including the presence of the rest of the glassy IGF on this adsorption, providing the mechanism for Lu adsorption that eluded all previous studies.

(g) In conjunction with (f), the importance of including the overlaying IGF on adsorption of specific rare-earths onto the crystal surface and the role of N and RE concentration was provided and showed the weakness in the ab-initio calculations of clusters or small system size.

1. Dissolution Behavior:

We have taken alumina crystals with two low energy surfaces, the (0001) basal plane (~2.0J/m^2) and the $(11\bar{2}0)$ prism surface (~2.5J/m^2) as the initial crystal orientations in contact

with the silicate IGFs. Previous work showed preferential adsorption and crystal growth along the surface normal on the $(11\bar{2}0)$ surface at certain IGF compositions, with slower growth on the basal orientation (which is consistent with experimentally observed anisotropic grain growth in alumina). However, at elevated temperatures, we expect preferential dissolution of the higher energy $(11\bar{2}0)$ surface into the silicate melt in comparison to the (0001) surface. To test this, we simulated crystal/vacuum interfaces followed by crystal/silicate melt interfaces to see the effect of T and melt composition on crystal surface stability.

Using a temperature at which both crystal orientations were stable in MD simulations of crystal/vacuum interfaces, simulations of these orientations in contact with silicate melts showed quite different results. Figure 1 shows a schematic of the system configuration. Figure 2 shows the number density of Al ions in the original crystals with the basal and prism orientations as well as those crystals in contact with two different silicate melts (no other ions shown in the figures). Arrow in each figure locates the original terminal Al plane in each crystal.

Figure 1

Al_2O_3 crystal	Silica or Silicate melt	vac

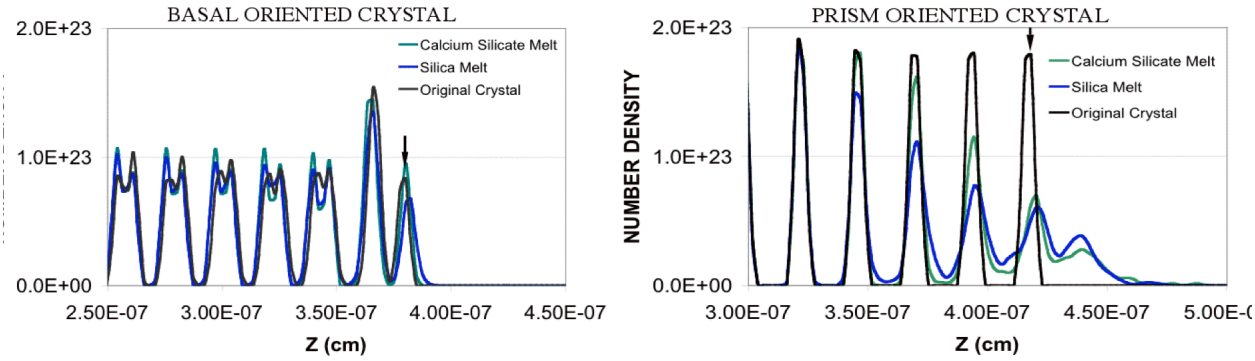

Figure 2. Al ion distribution in basal oriented crystal (left) and prism oriented crystal (right) in contact with melts.

Clearly, under the same conditions of melt composition and time at temperature, the (0001) basal surface remained stable for higher temperatures while the $(11\bar{2}0)$ prism surface showed dissolution into the melt. Therefore, during liquid phase sintering (LPS) at this

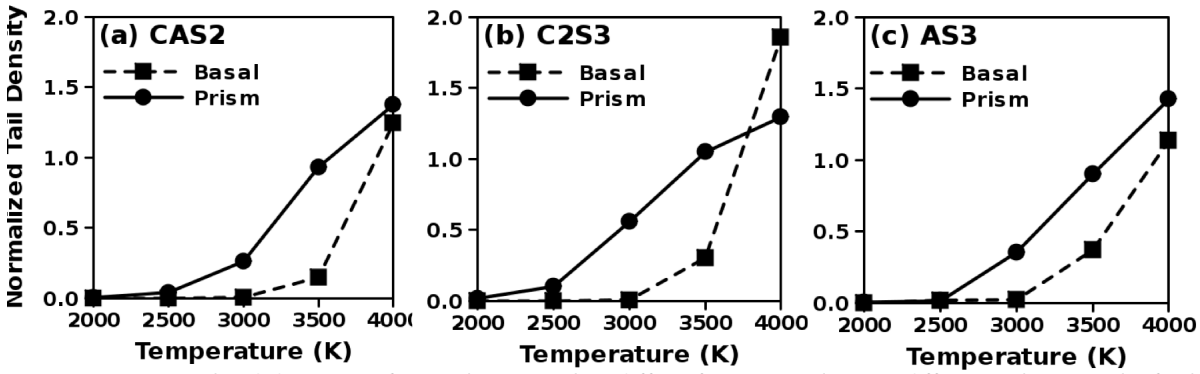

Figure 3. Normalized densities of crystal species that diffuse from crystal into 3 different silicate melts for basal and prism orientations (a) anorthite, (b) calcium silicate, (c) alumino-silicate. Significant anisotropic dissolution seen at T=3000K, with the prism less stable than the basal orientation.

equivalent temperature, the prism oriented surfaces preferentially dissolve into the silica(te) melts while the basal oriented surfaces are more stable. However, as our earlier work showed, at lower temperatures during cooling from the melt state, adsorption and growth on the prism surface occurs more rapidly than on the basal surface. Therefore, there are competing kinetics in LPS during which the prism surface dissolves, providing Al (and O) ions into the melt at certain temperatures, but preferentially grows at other lower temperatures and compositions. Additional studies of dissolution at different temperatures and melt compositions provided more specific information with respect to dissolution behavior. Figure 3 shows the density of species from the crystals that have dissolved into the different silicate melts as a function of temperature, clearly showing the significant anisotropy of dissolution at temperatures between 2500K and 3500K, with the most pronounced difference at 3000K, where the basal surface is stable and the prism surface dissolves into the melt.

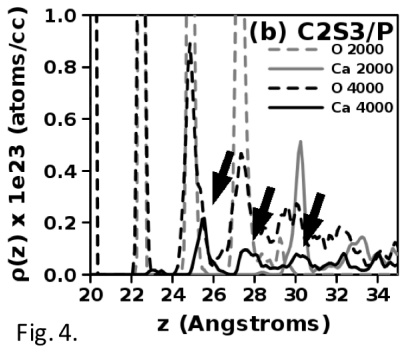

Fig. 4.

Another important feature observed in the simulations was the incorporation of Ca ions into the alumina prism surface as Al and O species migrated into the melt. This is seen in figure 4, with the arrows showing Ca peaks at broadened O peaks remaining in the crystal, suggestive of the formation of a calcium aluminate, which is known to occur in this system.

2. Fracture Behavior:

Fracture of IGF systems was accomplished by straining the sample in the direction perpendicular to the IGF/crystal interfaces, allowing for relaxation in the directions perpendicular to the strain direction. Film thickness has been shown in our simulations to affect fracture strength (figure 5a), with the SiO_2 IGF with a film thickness $\geq$ 2nm showing fracture similar to bulk amorphous silica (black rectangle) and thinner films showing increased fracture strength. Because of the role of 'void' formation and coalescence during fracture of bulk glasses,

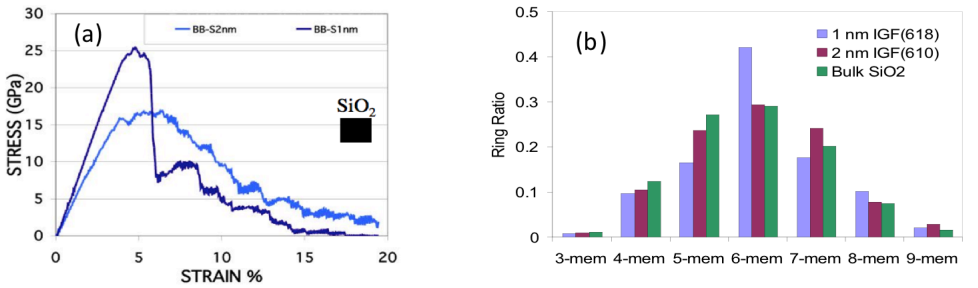

Figure 5. (a) Stress-strain results of IGFs and average data for silica fibers and simulation. Strain in IGFs is an artifac of using whole system dimension while only IGF takes all the strain. Correction puts strain near silica result. (b) Ring size distribution for IGFs and bulk silica showing major difference is in the 6-membered rings in the 1nm film.

we evaluated void formation in these confined films using analysis of the ring structures. Formation of larger rings implies larger 'voids' in the glass, with accompanying weakening of the material. The main difference between the 1nm IGF and the 2nm IGF is in the distribution of rings, especially in the concentration of 6 membered rings, as shown in figure 5b. Ring coalescence is seen in the images of the IGFs during strain. We were able to attribute this difference in strength to a significant increase in the concentration of 6-membered rings in the thinner IGF than the thicker IGF, giving the thinner IGF a characteristic more akin to crystalline

silica (predominantly 6-membered rings), which has a higher fracture strength than glassy silica. Interestingly, Doblinger et al. (Acta Mater. (2006)) mention experimental observation of increasing strength with decreasing IGF thickness, but do not discuss details.

Figure 6 shows the concentration of different ring structures *during* fracture of the 1nm film between silicon nitride crystals, as well as the stress (black line, given as 0.02*stress to fit on scale). Arrows point to (1) increase of very large 9-membered rings at first decrease in stress and (2) maximum stress followed by increase in 7- and 9-membered rings, plus increase in 3- and 4-membered rings (latter two structural features are consistent with formation of new surface), as well as a large decrease in 6-membered rings.

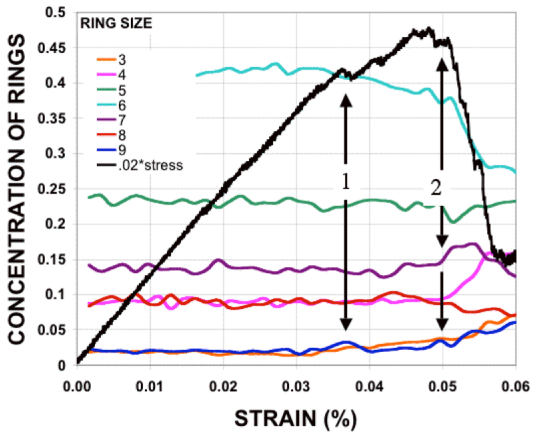

Figure 6. Variation in ring size distribution during fracture and rescaled stress-strain curve.

Our results show the **effect of composition** on maximum stress. Four additional features result from this work:

1. There is a change in the 'effective' composition of the glassy IGF caused by segregation of network modifiers (Ca in the current simulations) to the IGF/crystal interface that causes an increase in maximum stress. (This will have significant implications in IGFs containing both modifier ions and rare earth ions.)
2. Increased N (decreased O) in the IGF causes an increase in maximum stress, similar to experimental results.
3. Residual strain in the nitride crystal plays an important role in the calculated stress, affecting the interpretation of the resultant stress in the glassy IGF.
4. Allowing relaxation of the lateral dimensions (X and Y) at 1 atm pressure during imposed strain in Z results in a faster decrease in stress after the maximum stress with increasing strain. This indicates a more brittle nature to the IGF than would otherwise be inferred and is an important correction for those studies (eg. ab-initio calculations) that do not relax the lateral cell dimensions.

4. Variable Charge MD Simulations

We have incorporated variable charges on the ions based on the local configuration around the ion using the electronegativity equalization method and our newly developed iterative fluctuating charge algorithm. This enables a more accurate description of the charges on the ions, but requires modification of current parameters to allow for the correct exchange of charge between ions in the silicon nitride system.

5. Rare Earth Additions to IGF:

We added La and Lu rare earths (RE) to the IGFs to compare its behavior with that of Ca ions in IGFs between silicon nitride crystals. Ca ions preferentially segregate to the basal surface in alumina, but to the prism surface in the nitride (poisoning each and affecting adsorption and growth). Based on our knowledge of silicate glass structure and the role of 'modifiers' in silicate glasses, we can associate the adsorption of Ca ions onto certain sites on the prism oriented nitride

crystal that we see in our simulations to similar behavior of rare earth ions observed in HAADF-STEM. The use of La and Lu made the association between the simulations and the experiments more direct.

La Additions:

Initially, the interatomic potential for La additions in the silicon oxynitride IGF was developed and used in the silicon oxynitride IGFs. Figure 7 shows the locations of the La ions at the prism orientation of the Si_3N_4 crystal surface from (a) drawing from experiment shown in (b); (b) HAADF-STEM results by Winkelman et al, Mat. Sci. and Eng. A (2006); (c) our MD simulation results; (d) HAADF-STEM from a pocket. The drawing in (a) shows the predominant locations of the La ions at sites 1 and 2, plus sites 3 and 4, and are shown in the HAADF-STEM

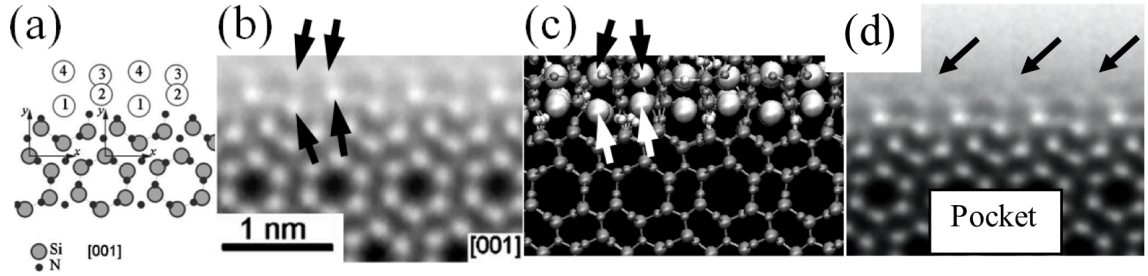

Figure 7. Four specific locations of La ions on the IGF/Prism interface viewed along the [001] direction, plus additional sites slightly visible in the pocket. (a) Drawing of La sites from Winkelman *et al.*; (b) HAADF-STEM image of IGF from Winkelman *et al.*; (c) our IGF MD simulation results; (d) HAADF-STEM of pocket. Arrows in (b) and (c) point out La sites 1, 2, 3, and 4 from experiments and simulations of IGF showing exact same multiple locations and in (d) show additional sites in thicker pocket.

at the black arrows, and which are consistent with the locations we observe in our simulations (black arrows).

The filling of these sites by the La ions varies with composition of the IGF, as shown in figure 8 (which includes La site-filling on the basal oriented surface also). The figure shows two important results regarding interface structure: (1) increasing La concentration allows for adsorption into sites 3 and 4, indicating ordered growth of La-X from the crystal into the IGF (and increased La order into the IGF increases strength), and (2) increasing N in the IGF causes much greater loss of site-filling on the basal surface than the prism (although both show losses in site adsorption). This greater loss on the basal surface provides a mechanism for faster growth along the surface normal (outward growth) of the basal surface than the prism surface consistent with anisotropic grain growth. With less La adsorbing on the basal surface, less poisoning occurs and greater anisotropy is expected (as seen experimentally).

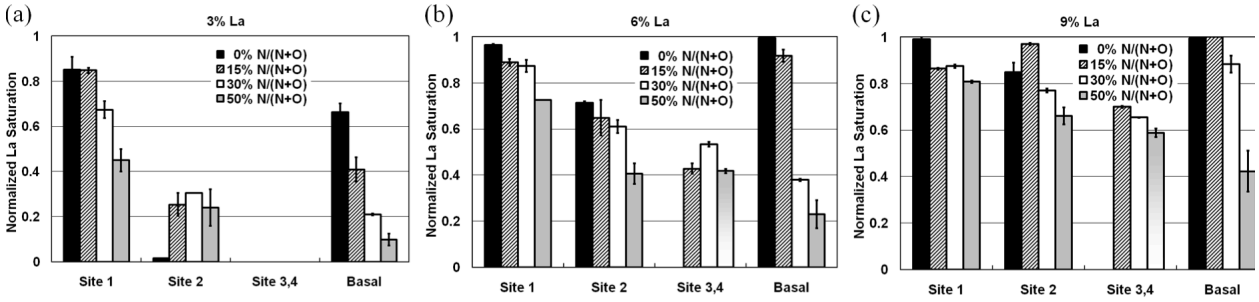

Figure 8. Normalized La saturation percentages of sites 1, 2, 3, 4 and basal for (a) 3% La, (b) 6% La, and (c) 9% La in 2nm IGFs. Error bars are drawn. Data of sites 3 and 4 for the 50%N/(N+O) cases are marked gradient gray because of the vague La ordering at sites 3 and 4.

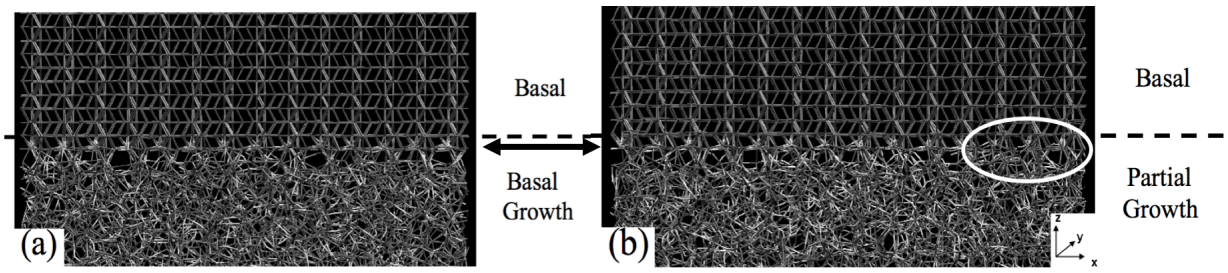

Figure 9. Snapshots of (a) basal growth (50N3La), and (b) partial basal growth (50N6La). Atoms not shown. Dashed lines are drawn to distinguish the original basal crystal and the new basal layer (at arrow). Ellipse is drawn in (b) to point out the region where basal growth does not occur, creating a step.

This growth of the basal surface as a function of La concentration is shown in figure 9a and b, with the arrow pointing to the extra layer of crystal that forms (uniformly in (a) and less so in (b), where in (b) the ellipse encircles an amorphous region that prevents crystal growth). This is remarkably relevant because the outward growth of the basal surface does not show a singular (flat) basal surface, but rather is slightly rounded, indicating partial growth regions, as would occur in the manner shown in 9(b). Our simulation results provide a mechanism for this physically observed growth behavior that has not been defined previously and shows the importance of the actual local composition.

We also show how the energies of the La ions vary in the glassy IGF interior versus the interface sites, showing the driving force for adsorption to interface sites as a function of composition.

Another important result is our study of 1.8nm and 0.6nm IGFs between prism and basal and prism and $(31\bar{4}1)$ oriented crystals (the latter combination mimics prism/IGF/misoriented crystal systems observed experimentally). The 0.6nm system reproduces the HAADF-STEM work done by Pennycook at ORNL on the same system sizes. Importantly, the 1.8nm systems show the ordering of the La at sites 1, 2, 3, 4, plus limited site filling at locations 5, and 6. The latter two sites, 5 and 6, are observed in pockets, but with low site filling (see fig 7d), showing the importance of the spacing of the 2nd crystal from the prism crystal on La ordering. *Ordering of La into the IGF has a significant effect on the strength of the IGF.*

An important difference in the La ordering occurs in the 1.8nm vs. the 0.6nm IGFs shown in figure 10. Not only are sites 5 and 6 missing in the 0.6nm IGF, but even sites 3 and 4 are missing in the 0.6nm IGF, while they remain in the 1.8nm film. Our results show that sites 3 and 4 are at a spacing that would impinge on the 2nd crystal at 0.6nm, significantly impeding or altering their formation. This is important because fracture occurs only in the glassy portion of the IGF, so extension of the ordered La sites increases strength, where the thinner IGF is

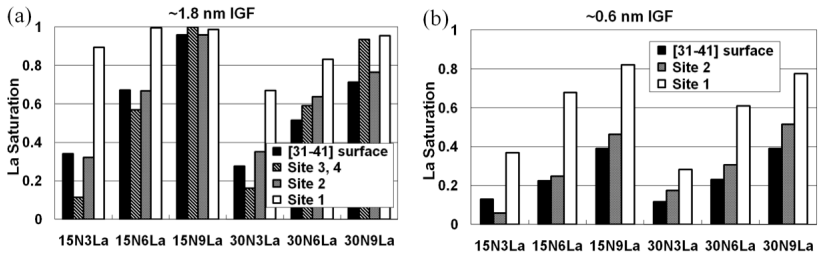

Figure 10. Comparison of La saturation percentage at various locations (La at site 1, 2, 3, 4 on the prism interface or on the $(31\bar{4}1)$ surface) for (a) ~1.8 nm IGF and (b) ~0.6 nm IGF of various compositions, showing the significant loss in site saturation with thinner IGFs at equivalent compositions. Sites 3 and 4 do not occur in the 0.6nm IGF.

weaker than the thicker one. This is opposite from the fracture data of the pure SiO_2 IGF discussed above and shows the importance of the exact local composition.

Lu Additions:

The addition of Lu ions to the IGF turned out to be far more difficult than originally expected, even though ab-initio calculations by Painter et al. (PRB 2008) should have alerted us since they also had problems in reproducing the HAADF-STEM results. Figure 11 a, b shows the location of Lu at the prism surface of silicon nitride at correct sites Lu1 and Lu2 based on HAADF-STEM analysis, in which the Lu' sites are incorrect. Lu1 was not reproduced in the ab-initio calculations but Lu1' was; La seen in (c), showing quite different siteing than Lu.

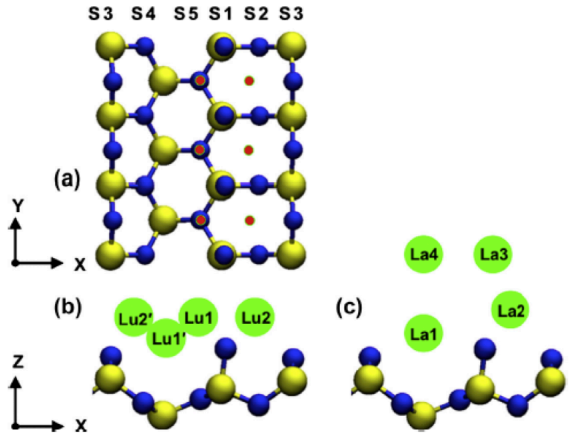

Figure 11 (a) Top view and (b, c) side view of the Si_3N_4 prism surface (N in blue spheres, Si in larger yellow spheres). Nitrogen sites are respectively labeled as S3, S4, S5, S1, S2, S3 along the x axis. The red dots in (a) indicate possible Lu1 and Lu2 sites. In (b) are shown Lu adsorption sites Lu1, Lu2, Lu1′ and Lu2′ (c) La adsorption sites La1, La2, La3 and La4 on the Si_3N_4 prism surface.

The simulations were able to reproduce the correct Lu siteing by incorporation of Oxygen into specific Nitrogen surface lattice sites (the blue colored N in figure 11 show the labels used for these N surface sites). The simulations showed that exchange of N-sites S1 alone or with other N sites resulted in the correct adsorption of Lu on the prism surface. The presence of O at these surface N sites was observed in EELS analysis of the prism surface by Walkosz et al. (PRB 2010). An important feature is that, while ab-initio calculations also replaced site S1 with O, the correct siteing was not attained (PRB 2008). We believe that this is due to the fact that the ab-initio calculations did not include the rest of the IGF in their calculations, whereas our MD simulations did include the IGF. This overlayer of the IGF plus the presence of O at N surface sites allowed for the correct results. Additional simulations showed the energy of Lu adsorption onto the different surface locations, showing the lowest energy sites at Lu2 and Lu1, as anticipated from HAADF-STEM. Figure 12 shows this surface energy profile and the role of a pre-adsorbed Lu onto Lu2 (grey), the repulsive regime around this site (brown), and the low energy sites Lu1 and Lu2, which provides the

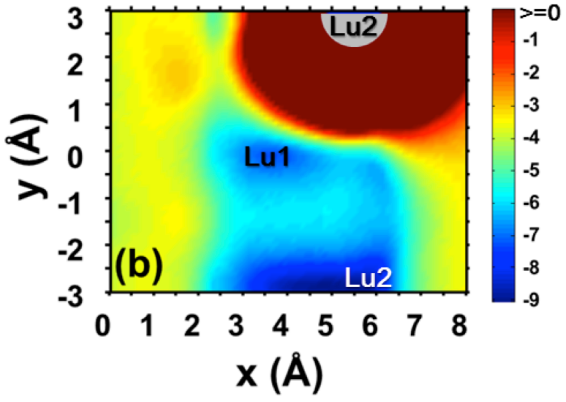

Figure 12. Energy map for Lu on the prism surface with O at the S1 sites. Grey hemisphere at (5.5, 3) is one Lu at site Lu2 that is kept frozen, while a second Lu samples the rest of the adjacent surface sites. Site Lu1 is at (3.5, 0) and a second Lu2 site at (5.5, -3). Color bar gives Lu energy in eV.

mechanism of the staggered siteing of Lu at different x-positions along row y in figure 11a.

Growth behavior of La- and Lu-doped IGFs:

The effect of Lu in the IGF on growth is shown in figure 13 in comparison to the lack of growth of the prism surface when the IGF contains La. Even though both La and Lu are seen at room temperature in HAADF-STEM, La has a much greater role in poisoning the prism surface

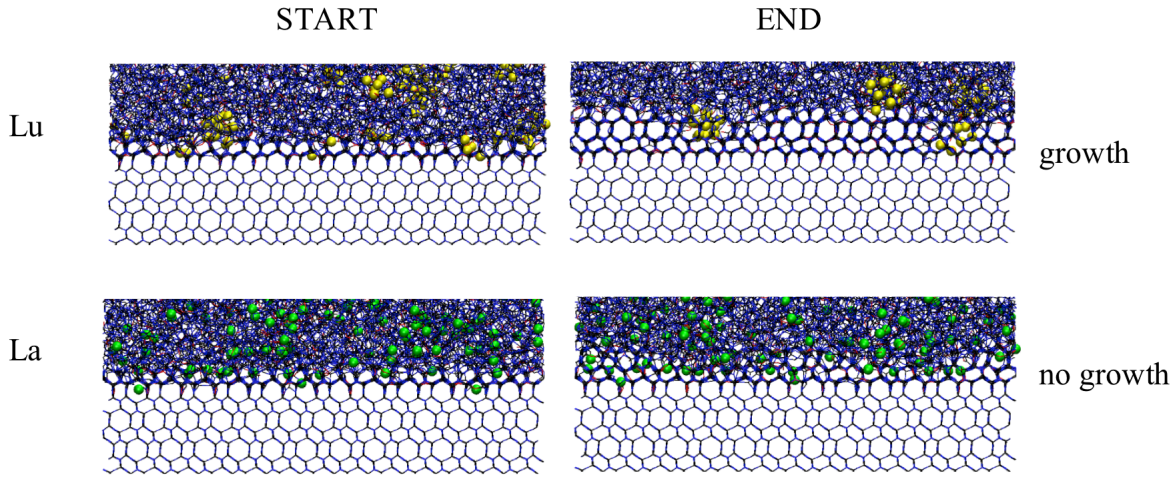

Figure 13. Effect of Lu (top) and La (bottom) in the IGF on growth of the prism surface at the start and end of the run at elevated temperature.

than Lu. While the elevated temperature results in figure 13 show the increased growth of the Lu exposed prism surface, the presence of Lu at the crystal surface seen in HAADF-STEM at room temperature is not explained. However, the explanation can be obtained from the data in figure 14, in which the density profiles of the various species in the crystals (left and right of the

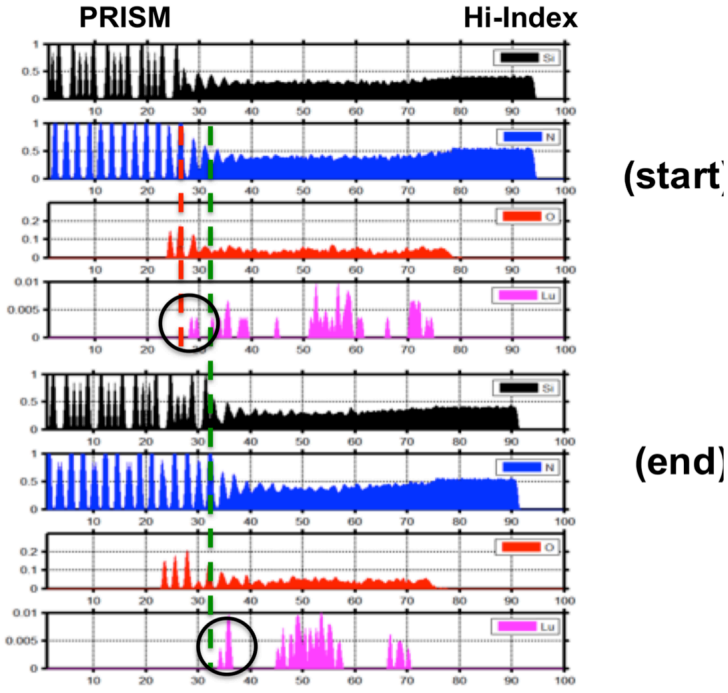

Figure 14. Density profiles of species in crystals and IGF as a function of distance perpendicular to the crystal/IGF interfaces. Crystal grows from red dashed vertical line in (start) to green dashed vertical line at (end), with Lu present at the surface in both locations (black circles). This shows that Lu is less strongly bound to the crystal surface, allowing for growth, but nonetheless is present during and after growth so that it is seen at the surface in HAADF-STEM.

images) and the IGF at the start and end of a high temperature run are shown. The Lu moves away from the growing surface, but remains close even at the high temperature. Growth can occur, even though at room temperature HAADF-STEM images show the Lu still present, in which one could incorrectly infer Lu's possible role as a poison for growth. La does not show this behavior. Therefore, the simulations show that Lu does not adhere to the surface at the sintering temperatures and thus enables growth of the crystal, providing the explanation for its presence in HAADF-STEM without the deleterious effects afforded by La on poisoning growth.

6. Equilibrium Structures and Compositions:

Rather than using the extremely computationally intensive grand canonical approaches to studying these very compositionally complex multicomponent systems (whose ion charges and bond directionality impose serious constraints in the GC methods), we are extending the ADF method to address equilibrium behavior in IGFs. ADF offers the potential of more rapid equilibration of a liquid phase into the space between crystals than would be possible with MD simulations or even GCMD. As mentioned above, we are using a known interatomic potential with a softened core in the ADF equations rather than using a phenomenological free energy functional form. Our approach is designed to allow us to incorporate existing interatomic potentials into the ADF format, thus connecting directly to previous and further MD simulations. We have begun using simple pair potentials to develop code and methodology, with plans to move to our more realistic multibody potentials that describe our systems. Figure 14 shows the evolution of a polycrystalline system with our approach at different reduced temperatures and times. Results show grain growth and removal of curved boundaries and small grains as a function of time and temperature.

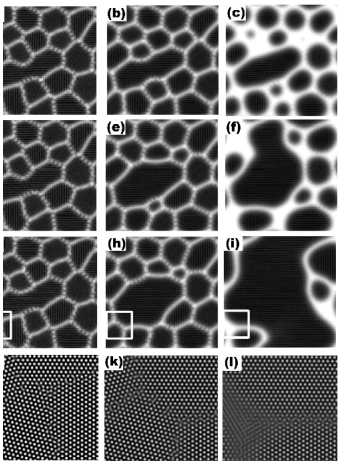

Figure 14. Free energy maps of annealed polycrystalline samples (a-i) and atomic density maps (j-l). From the leftmost column, $T^* = 0.5$, $T^* = 0.55$, and , $T^* = 0.56$, respectively; from the top row, averaged energy at time $\tau = 1$, 1.5, and 2.5, respectively, and atomic density (boxed area in energy maps at $\tau = 2.5$). The free energy is smoothed by averaging the free energy in $r < r_{out}$ range. Higher F^* is presented as brighter color, and the brightness of each temperature conditions is adjusted to contrast the high energy sites (i.e. dislocations and grain boundaries).

STUDENTS AND POST-DOCTORAL RESEARCHER SUPPORTED:

Graduate Students: Yun Jiang (100%), Glenn Lockwood (10%), Shenghong Zhang (100%).
Post-Doc: Dr. Ying Ma (10%), Dr. Jihee Kim (100%)
Undergraduate students: N. Michaluk (100%), P. Kent(100%), N. Twu(100%).

INVITED LECTURES RELATING TO THIS PROJECT:

Electronic Materials and Applications: Basic Science Div. Am. Ceram. Soc. Orlando, 2014

Lawrence Livermore National Laboratory, Computational Chemistry and Materials Sci. Institute, 2013

Materials Science and Technology Annual Mtg, Interface Symposium, Columbus OH, 2011

Materials Science and Technology Annual Mtg, Grain Boundary Symposium, Columbus OH, 2011

Clemson University, Dept. Matl. Sci. and Eng., SC, 2011

International Workshop on Interfaces, PA, 2009

MS&T Annual Meeting, Detroit MI, 2007

University of California, Davis, CA, 2007

TMS Annual Meeting, Orlando, FL, 2007

Lehigh University, Materials Science and Engineering, PA, 2006

Interfaces in Functional Ceramics and Glass/Ceramics: Theory to Experiment, PA, 2006

PUBLICATIONS

"Role of oxygen on the interfacial adsorption sites of Lu and La in β-Si_3N_4", Y. Jiang, Y. Ma, and S. H. Garofalini, Acta Mater. 66 (2014) 284-292. (exclusively acknowledges THIS GRANT support)

"Effect of thickness and composition on the structure and ordering in La-doped intergranular films between Si_3N_4 crystals", Y. Jiang and S. H. Garofalini, Acta Mater. 59 (2011) 5368-5377. (exclusively acknowledges THIS GRANT support)

"Order in nanometer thick intergranular films at Au-sapphire interfaces", M. Baram, S. H. Garofalini and W. D. Kaplan, Acta Mater. 59 (2011) 5710-5715. (exclusively acknowledges THIS GRANT support for SHG, other two authors supported by Israel Science Foundation)

INVITED PAPER in THEMED ISSUE: "Molecular Dynamics Simulations of La_2O_3-doped Silicate Intergranular Films in Si_3N_4", Y. Jiang and S. H. Garofalini, J. Matl. Chem. 20 (2011) 10359-10365. (exclusively acknowledges THIS GRANT support)

"Molecular dynamics simulations of the effect of the composition of the intergranular film on fracture in Si_3N_4", S. H. Garofalini and S. Zhang, J. Am. Ceram. Soc. 93 (2010) 235-240. (exclusively acknowledges THIS GRANT support)

"Molecular Dynamics Simulations of the Locations of La Ions in La-Si-O-N Intergranular Films in Silicon Nitride", Y. Jiang and S. H. Garofalini, J. Am. Ceram. Soc. 93 (2010) 3886-3892. (exclusively acknowledges THIS GRANT support)

"Effect of thickness of the intergranular film on fracture in Si_3N_4", S. Zhang, and S. H. Garofalini, J. Am. Ceram. Soc.92 (2009)147-151. (exclusively acknowledges THIS GRANT support)

"Anisotropic dissolution of α-alumina (0001) and $(11\bar{2}0)$ surfaces into adjoining silicates", G. K. Lockwood, S. Zhang, and S. H. Garofalini, J. Am. Ceram. Soc., 91 (2008) 3536-3541. (exclusively acknowledges THIS GRANT support)

"Molecular dynamics simulations of beta-SiC using both fixed charge and variable charge models", Y. Ma and S. H. Garofalini, J. Chem. Phys., 128 (2008) 084505. (exclusively acknowledges THIS GRANT support)

"Modeling of microstructural evolution using atomic density function and effective pair potentials", J. Kim and S. H. Garofalini, Phys. Rev. B 78 (2008) 144109 (exclusively acknowledges THIS GRANT support)

"Role of Lu and La in the intergranular films on growth of the prism surface in β-Si_3N_4: A Molecular Dynamics Study", Y. Jiang and S. H. Garofalini, J. Am. Ceram. Soc. (submitted) (exclusively acknowledges THIS GRANT support